

Summertime diurnal variations in the isotopic composition of atmospheric nitrogen dioxide at a small midwestern United States city

Wendell W. Walters^{a,*}, Huan Fang^a, Greg Michalski^{a,b}

^a Department of Earth, Atmospheric, and Planetary Sciences Purdue University, 550 Stadium Mall Drive, West Lafayette, IN, 47907, United States

^b Department of Chemistry, Purdue University, 560 Oval Drive, West Lafayette, IN, 47907, United States

ARTICLE INFO

Keywords:

Nitrogen
Nitrogen oxides
Isotopes
Atmospheric emissions
Oxidation

ABSTRACT

The nitrogen and oxygen stable isotopes ($\delta^{15}\text{N}$ & $\delta^{18}\text{O}$) of nitrogen oxides ($\text{NO}_x = \text{nitric oxide (NO)} + \text{nitrogen dioxide (NO}_2\text{)}$) may be a useful tool for partitioning NO_x emission sources and for evaluating NO_x photochemical cycling, but few measurements of *in situ* NO_x exist. In this study, we have collected and characterized the diurnal variability in $\delta^{15}\text{N}$ and $\delta^{18}\text{O}$ of NO_2 from ambient air at a small Midwestern city (West Lafayette, IN, USA, 40.426° N, 86.908° W) between July 7 to August 5, 2016, using an active sampling technique. Large variations were observed in both $\delta^{15}\text{N}(\text{NO}_2)$ and $\delta^{18}\text{O}(\text{NO}_2)$ that ranged from -31.4 to 0.4% and 41.5 – 112.5% , respectively. Daytime averages were $-9.2 \pm 5.7\%$ ($\bar{x} \pm 1\sigma$) and $86.5 \pm 14.1\%$ ($n = 11$), while nighttime averages were $-13.4 \pm 7.3\%$ and $56.3 \pm 7.1\%$ ($n = 12$) for $\delta^{15}\text{N}(\text{NO}_2)$ and $\delta^{18}\text{O}(\text{NO}_2)$, respectively. The large variability observed in $\delta^{15}\text{N}(\text{NO}_2)$ is predicted to be driven by changing contributions of local NO_x emission sources, as calculated isotope effects predict a minor impact on $\delta^{15}\text{N}(\text{NO}_2)$ relative to $\delta^{15}\text{N}(\text{NO}_x)$ that is generally less than 2.5% under the sample collection conditions of high ozone concentration ($[\text{O}_3]$) relative to $[\text{NO}_x]$. A statistical $\delta^{15}\text{N}$ mass-balance model suggests that traffic-derived NO_x is the main contributor to the sampling site (0.52 ± 0.22) with higher relative contribution during the daytime (0.58 ± 0.19) likely due to higher traffic volume than during the nighttime (0.47 ± 0.22). The diurnal cycle observed in $\delta^{18}\text{O}(\text{NO}_2)$ is hypothesized to be a result of the photochemical cycling of NO_x that elevates $\delta^{18}\text{O}(\text{NO}_2)$ during the daytime relative to the nighttime. Overall, this data suggests the potential to use $\delta^{15}\text{N}(\text{NO}_2)$ for NO_x source partitioning under environmental conditions of high $[\text{O}_3]$ relative to $[\text{NO}_x]$ and $\delta^{18}\text{O}(\text{NO}_2)$ for evaluating $\text{VOC-NO}_x\text{-O}_3$ chemistry.

1. Introduction

Nitrogen oxides ($\text{NO}_x = \text{nitric oxide (NO)} + \text{nitrogen dioxide (NO}_2\text{)}$) play a key role in controlling the concentrations of atmospheric oxidants that drive tropospheric chemistry (Crutzen, 1973, 1979; Leighton, 1961; Logan, 1983). Photochemical reactions involving NO_x , carbon monoxide, and volatile organic compounds (VOC) lead to the formation of tropospheric ozone (O_3), which is a greenhouse gas, an oxidizing pollutant, and influences the lifetimes of other greenhouse gases (Atkinson, 2000; Atkinson and Arey, 2003; Crutzen, 1979). Photochemical cycling involving NO_x and reduced hydrogen oxide radicals ($\text{HO}_x = \text{hydroxyl radical (OH)} + \text{peroxy radicals (HO}_2\text{ and RO}_2\text{)}$) is terminated when NO_2 is further oxidized to nitric acid (HNO_3). Once HNO_3 is formed, it is primarily removed via wet and/or dry deposition leading to degradation of drinking water, soil acidification, eutrophication, and biodiversity change in terrestrial ecosystems (Galloway et al., 2004). Thus, due to the environmental and human

health consequences of NO_x and its oxidation products, it is important to understand the relative contributions of NO_x emission sources and the oxidation processes responsible for its removal.

Sources of NO_x are both of natural (e.g. lightning, soil nitrification/denitrification, and wildfires) and anthropogenic (e.g. fossil fuel combustion, industry, and agriculture) origins (Galloway et al., 2004; Jaeglé et al., 2005; Reis et al., 2009), but there are uncertainties in the temporal and spatial contributions of various emission sources that might be resolved by nitrogen (N) stable isotope analysis ($\delta^{15}\text{N}$). Numerous studies have quantified the difference in $\delta^{15}\text{N}$ values of various NO_x sources, which indicate relative distinctive values for biogenic NO_x (nitrification/denitrification), the transportation sector, and coal-fired power plants (Ammann et al., 1999; Felix et al., 2012; Felix and Elliott, 2013; Fibiger et al., 2014; Heaton, 1987, 1990; Hoering, 1957; Li and Wang, 2008; Miller et al., 2017; Moore, 1977; Snape et al., 2003; Walters et al., 2015a, 2015b). These isotopic “fingerprints” may be a useful tool for constraining the NO_x emission budget; however, it is

* Corresponding author.

E-mail address: waltersw@purdue.edu (W.W. Walters).

¹ Present address: Department of Earth, Environmental, and Planetary Sciences, Brown University, 324 Brook Street, Providence, RI, 02912, United States.

difficult to collect *in situ* NO_x for isotopic characterization because it is highly reactive and has low mixing ratios. Thus, numerous studies have inferred δ¹⁵N(NO_x) values from the δ¹⁵N of atmospheric nitrate, which is easier to collect and isotopically analyze. However, any attempt to partition NO_x sources using the δ¹⁵N values of atmospheric nitrate may be complicated by possible kinetic (Freyer, 1991; Walters and Michalski, 2016a), equilibrium (Walters and Michalski, 2015, 2016b), and photolytic isotope effects that occur during the oxidation of NO_x to atmospheric nitrate. For example, previous works have suggested isotopic exchange between NO and NO₂ (Freyer et al., 1993; Walters et al., 2016) might alter δ¹⁵N(NO₂) values relative to δ¹⁵N(NO_x), which may then be propagated into the δ¹⁵N value of atmospheric nitrate (Riha, 2013; Savarino et al., 2013). Therefore, it is still unclear at locations with multiple significant NO_x emission sources if δ¹⁵N(NO₂) reflects NO_x emission sources, chemistry effects, or a combination of these processes. It is important to understand drivers of δ¹⁵N(NO₂) since NO₂ is precursor to atmospheric nitrate.

The analysis of the oxygen (O) stable isotope composition (δ¹⁸O) of NO_x and atmospheric nitrate may trace NO_x photochemical cycling and be an evaluator of changing daytime and nighttime oxidation chemistry (Michalski et al., 2003, 2014, 2012; Morin et al., 2008). Prior experimental investigations suggest that O isotopic equilibrium is achieved between NO_x and O₃ (Michalski et al., 2014), erasing the original NO_x source O isotopic composition. Atmospheric O₃ has a characteristically elevated δ¹⁸O values of ≈100‰ (Johnston and Thiemens, 1997; Krankowsky et al., 1995; Mauersberger et al., 2001; Thiemens and Heidenreich, 1983; Vicars et al., 2012; Vicars and Savarino, 2014), and the coupling between NO_x and O₃ in the Leighton Cycle is believed to be the driver of high δ¹⁸O observed in atmospheric nitrates (Michalski et al., 2003; Morin et al., 2008; Savarino et al., 2008). An experimental study of NO-O₂-O₃-NO₂ photochemical equilibrium under tropospheric conditions predicts δ¹⁸O(NO_x) of 117 ± 5‰ relative to Vienna Standard Mean Ocean Water (VSMOW) (Michalski et al., 2014), but this appears at odds with recent *in situ* measurements (Dahal and Hastings, 2016; Felix and Elliott, 2014). The δ¹⁸O values of NO₂ measured using passive diffusion collectors was found to range from 47.3 to 54.6‰ at an urban location (Providence, RI, USA) (Dahal and Hastings, 2016) and from -21.5–37.8‰ at sample sites near NO_x emission sources (tunnel, fertilized soil emissions, livestock waste facilities) (Felix and Elliott, 2014), which are significantly lower than the model predictions (Michalski et al., 2014). The apparent disagreement between the measured and expected δ¹⁸O value of *in situ* NO_x may be attributed to possible O isotopic fractionation associated with the collection of NO₂ (i.e. conversion of NO₂ to nitrite (NO₂⁻)) on passive diffusion pad or O isotopic exchange between NO₂⁻ and water during storage (Dahal and Hastings, 2016), influences from O isotopic signatures from NO_x emissions sources (Felix and Elliott, 2014), or photochemical non-equilibrium with O₃. Thus, δ¹⁸O value of *in situ* NO_x remains uncertain and likely highly variable and what that variations means in terms of photochemical oxidation pathways still requires resolution.

To improve our understanding of the N and O isotopic composition of NO_x, separate daytime and nighttime isotopic measurements of *in situ* NO_x are required. In this study, the diurnal variations in δ¹⁵N and δ¹⁸O values of *in situ* NO₂ was measured using an active sampling technique, and the data was evaluated in the context of source and chemical isotope effects with the goal of understanding the drivers of δ¹⁵N and δ¹⁸O variabilities in NO₂.

2. Methods

2.1. Sampling location

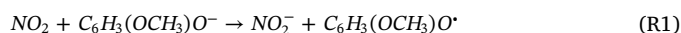
NO₂ was collected from ambient air on the rooftop of a building (Hampton Hall of Civil Engineering) on the campus of Purdue University (West Lafayette, IN, USA, 40.426° N, 86.908° W) (Fig. 1) [Google Earth, 2016]. The surrounding land-use is the urban/sub-urban

sister cities of Lafayette-West Lafayette, IN that have a combined population of roughly 150,000. The sampling location was approximately 12 m above ground and was directly above a loading dock with light daytime diesel truck and gasoline vehicle traffic and approximately 50 m from a regularly traveled road that experiences moderate weekday rush hour traffic at approximately 7–8 a.m. and 5–6 p.m. The 2011 U.S. EPA emission inventory estimates the following yearly NO_x emission budget for the county of the sampling location (Tippecanoe): Mobile = 59.4%, Fuel Combustion = 35.3%, Biogenic = 4.2%, Industry = 0.7%, Waste = 0.3%, and Fire = 0.1% [Office of Air Quality Planning and Standards (2011)]. To the north and west of the sampling location is mostly roads, a golf course, and agricultural fields (maize and soybean). Approximately 2 km south of the sampling site is a 41.4 MW electrical-heat cogeneration plant that operates 3 natural gas and 1 coal-fired boilers.

2.2. *In situ* NO₂ collection

NO₂ was collected using a denuder tube active sampling apparatus (Fig. 2). Briefly, ambient air was drawn through a borosilicate tube (inner diameter = 3 mm and length = 1 m) using an air sampling pump flow controlled to 1 L/min. Based on the Gormley-Kennedy solutions for a cylindrical denuder (Ali et al., 1989), our sample flow rate, and an NO₂ diffusion constant of 1.36 × 10⁻⁵ m²/s at 273 K and 1 atm (Massman, 1998), NO₂ should be nearly 100% removed within 50 cm assuming a perfect NO₂ absorber. Our denuder tube should therefore provide roughly 2 times the length required for complete NO₂ absorption. As a quality control check, a second denuder tube was connected in series with the first tube to check for NO₂ breakthrough. The denuder tubes were held vertically to prevent gravitational sedimentation of < 1 μm particulate matter to the tube wall as an extra precaution (Ali et al., 1989). Prior to the denuder tube, a Millipore Fluoropore membrane filter (9 mm diameter) removed fine particulate matter > 1 μm. Particulates were removed before NO₂ because we did not have a denuder transition section to establish laminar flow. Therefore, turbulent flow at the beginning of our denuder tube could collect particulates, such that we opted to remove particles upstream of the denuder. In this set-up, it is possible that NO₂ may have reacted with particulates prior to NO₂ reaching the denuder, but the particulate filter was replaced each sampling period to not allow for excessive particulate buildup to minimize this possibility. All connections between the various components of the sampling apparatus was made using 1/4" Teflon tubing and ultratorr fittings. The sampling inlet (1/4" Teflon tubing) was mounted on the side of a building and sheltered from precipitation and direct sunlight.

The denuder tubes were coated with 0.5 mL of a 2.5 M potassium hydroxide, 25% by weight guaiacol (C₇H₈O₂), and methanol solution and dried with high-purity argon. The denuder tubes were prepared daily and used for NO₂ collection within 24 h. The guaiacol/KOH coating reacts with NO₂ to form NO₂⁻ (Ammann et al., 1999; Buttini et al., 1987; Li and Wang, 2008; Williams and Grosjean, 1990). Briefly, NO₂ undergoes an electron transfer reaction with deprotonated guaiacol (C₆H₃(OCH₃)O⁻) (Ammann et al., 2005), which is the preferential guaiacol product (pK_a = 9.98 (Pearce and Simkins, 1968);) under basic conditions (R1):



Previous studies have found that the guaiacol/KOH coating results in the bound NO₂ as NO₂⁻ with a stoichiometric factor of one (Buttini et al., 1987). From a mass-balance perspective, the N and O atoms in the NO₂⁻ product derive entirely from the atoms of the bound NO₂. Thus, the guaiacol/KOH coating provides a promising NO₂ concentration method for conserving both the N and O isotope signatures of atmospheric NO₂.

Other gaseous oxidized forms of nitrogen might interfere with the collected NO₂. High oxidized N forms such as N₂O₅ and HNO₃ should



Fig. 1. Aerial view of the area near the sampling site. The location of sampling site is indicated by the star and the location of the nearby utility plant (3 natural gas boilers and one coal-fired boiler) is indicated by the diamond. Image from Google Earth.

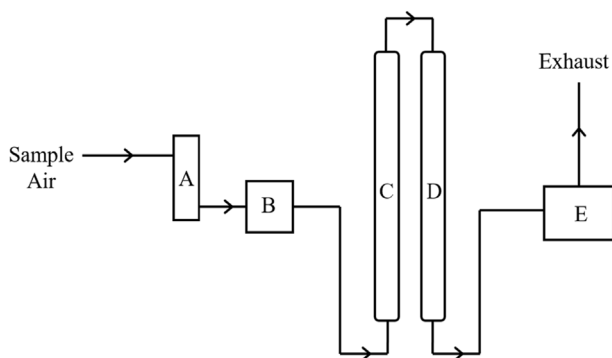


Fig. 2. Sampling apparatus schematic for collection of atmospheric NO_2 , where A is the flow meter (1 L/min), B is aerosol filter, C is the NO_2 binding denuder tube, D is the NO_2 breakthrough denuder tube, and E is the air sampling pump.

not have a major impact on our collected NO_2 since presumably these molecules will bind as NO_3^- , while our analysis is selective towards NO_2^- (see section 2.3). Other N oxidized forms that include peroxyacetyl nitrate (PAN) and nitrous acid (HONO) may, however, bind as NO_2^- (Buttini et al., 1987). PAN should not be an interference because it usually has very low concentrations at ambient temperature and previously found not to bind with the guaiacol/KOH coating (Buttini et al., 1987). HONO has been found to bind with the guaiacol/KOH coating as NO_2^- (Buttini et al., 1987), but interference is expected to be small because [HONO] is generally much lower than $[\text{NO}_2]$ by a factor of 10–20 (Harris et al., 1982). Thus, we did not remove HONO before collection of NO_2 , because coatings designed for HONO collection (i.e. sodium carbonate (Febo et al., 1993);) can also bind NO_2 with an efficiency as high as 28% (Williams and Grosjean, 1990), which may interfere with our results more than not removing the present HONO.

Ambient air was sampled separately during the daytime (~6 h) and nighttime (~8 h) during weekdays from July 7 to August 4, 2016. Daytime and nighttime collections typically occurred between 8:30 a.m. to 4:00 p.m. and 9:30 p.m. to 5:30 a.m., respectively (Table S1). NO - NO_2 - NO_x concentrations were measured using a Thermo Scientific NO_x 43C analyzer. After collection, the denuder tubes were separately rinsed with 3 mL of 18.2 M Ω Millipore Water. NO_2^- test strips

(AquaChek[®]) were used as a semi-quantitative check for $[\text{NO}_2^-]$ and was found to always test positive for the capture denuder and negative for the breakthrough denuder. Thus, the eluent from the second denuder tube was discarded and the eluent from the first denuder tube was immediately placed in a freezer until isotopic analysis. As a quality control check of our data, we estimate collection yield for each sample based on peak yields from isotopic analysis (see below) compared to the expected amount that was determined from the integrated $[\text{NO}_2]$ measured using the Thermo Scientific NO_x 43C analyzer. This was the chosen method rather than $[\text{NO}_2^-]$ quantification using Ion Chromatography or colorimetric analysis because (1) we were generally sample-limited and needed all collected sample for isotopic analysis and (2) we found the denuder extraction matrix to impede with the colorimetric determination of $[\text{NO}_2^-]$ (e.g. US EPA Method 353.2), such that it was difficult to analyze low $[\text{NO}_2^-]$ samples because of relatively low precision ($\pm 5 \mu\text{M}$).

2.3. Isotopic analysis of NO_2

Isotopic analysis ($\delta^{18}\text{O}$ & $\delta^{15}\text{N}$) was performed on the product NO_2^- in the frozen eluent extracted from the first denuder tube. Samples were left out at room temperature to thaw approximately 2 h before the analysis. The entire eluent of approximately 3 mL from each sample was converted into nitrous oxide (N_2O) using sodium azide in an acetic acid buffer (McIlvin and Altabet, 2005). The product N_2O was extracted and purified using an automated headspace gas chromatography system and analyzed by a Thermo Delta V Continuous Flow Isotope Ratio Mass Spectrometer for m/z 44, 45, and 46 at the Purdue Stable Isotopes Lab. Measured $\delta^{15}\text{N}$ (relative to air N_2) and $\delta^{18}\text{O}$ (relative to VSMOW) was calibrated to KNO_3 salts that included RSIL-N7373, RSIL-N23, RSIL-10219 assuming the following respective ($\delta^{15}\text{N}(\text{‰})$, $\delta^{18}\text{O}(\text{‰})$) values: (-79.6, 4.5), (3.7, 11.4), and (2.8, 88.5) (Böhlke et al., 2007). Direct calibration of our NO_2^- samples to NO_2^- standards, and the direct conversion of NO_2^- to N_2O using the sodium azide method (McIlvin and Altabet, 2005), allows us to ignore the uncertainty in correcting for isotopic fractionation of $\delta^{18}\text{O}$ using typical nitrate isotopic reference materials (Casciotti et al., 2007).

The NO_2^- samples typically contained between 30 and 125 nmoles of NO_2^- based on the product N_2O yield. Linearity effects were

corrected by using variable NO_2^- amounts of the standards that ranged between 20 and 250 nmoles. The isotopic precision was found to be highly dependent on the amount of NO_2^- analyzed. Near our sample sizes of 30–125 nmoles, the average standard deviation between the residual values of the calibrated standards for $\delta^{15}\text{N}$ and $\delta^{18}\text{O}$ was 1.1‰ and 0.6‰, respectively. This uncertainty is slightly higher than our usual isotopic precision for $\delta^{15}\text{N}$ and $\delta^{18}\text{O}$ of 0.6‰, and 0.4‰ that is found at NO_2^- amounts greater than 200 nmoles. Thus, we report $\delta^{15}\text{N}(\text{NO}_2)$ and $\delta^{18}\text{O}(\text{NO}_2)$ “raw measurement” errors of $\pm 1.1‰$ and $\pm 0.6‰$. Additionally, since our NO_2 samples are of atmospheric origin, $\delta^{15}\text{N}$ was also approximately corrected for N_2O isobaric influences from $\Delta^{17}\text{O}$ (Hastings et al., 2003). Unfortunately, we did not have enough sample for $\Delta^{17}\text{O}$ analysis, such that we estimated this value based on the measured $\delta^{18}\text{O}(\text{NO}_2)$ and assuming a mixing line between RO_2 ($\delta^{18}\text{O} = 23‰$, $\Delta^{17}\text{O} = 0‰$; (Michalski et al., 2012)) and terminal O atom of O_3 ($\delta^{18}\text{O} = 126.3‰$ and $\Delta^{17}\text{O} = 39.3‰$; (Vicars and Savarino, 2014), which are the oxidants responsible for oxidizing NO. This typically resulted in a small $\delta^{15}\text{N}$ correction of $-3‰$ during the daytime and $-1.5‰$ during the nighttime.

2.4. Control tests

Previous control tests demonstrated the robustness for characterizing $\delta^{15}\text{N}(\text{NO}_2)$ using the same denuder tubes employed in this study, with an isotopic precision of approximately $\pm 0.7‰$ (near our analytical precision) (Walters et al., 2016). Additionally, it was found that NO is not removed by the guaiacol/KOH denuder coating (Walters et al., 2016). To assess the precision of our sampling technique for $\delta^{18}\text{O}(\text{NO}_2)$, further control tests were conducted by flowing an aliquot of air from an NO_2 bulb through our sampling apparatus (Fig. 2). Isotopic analysis of the product NO_2^- resulted in $\delta^{18}\text{O}$ of $-1.8 \pm 1.2‰$ ($n = 7$), which indicates excellent precision; however, the $\delta^{18}\text{O}$ value of the NO_2 bulb is unknown. Since nearly 100% of NO_2 appears to bind on the denuder tube, $\delta^{18}\text{O}$ fractionation due to incomplete NO_2 collection should not be of concern. Assuming $\delta^{18}\text{O}(\text{NO}_2)$ is conserved as it is bound as NO_2^- , the major concern with preserving the $\delta^{18}\text{O}$ composition during sample storage is the possible O isotopic exchange of NO_2^- with water once eluted from the denuder tube. The elutant has a $\text{pH} > 10$, so that $\delta^{18}\text{O}$ exchange with water should be minimal (Casciotti et al., 2007). This was tested by periodically injecting 20–50 nmoles of a standard KNO_2^- salt (RISL-N10219) into the eluted guaiacol/KOH mixture over a period of one month. The controls were immediately placed in a freezer until isotopic analysis as performed in our collection of *in situ* NO_2 . Our control tests indicate that O isotopic exchange between NO_2^- and H_2O does occur in our samples, reaching approximately 3.5% within the first three days, based on a laboratory water $\delta^{18}\text{O}$ of $-8‰$ (Fig. 3). After this initial exchange, no further exchange in $\delta^{18}\text{O}$ was observed, as all control samples that were kept in solution between 3 and 31 days prior to isotopic analysis indicated an average O exchange with water of $2.7 \pm 2\%$ (Fig. 3). This consistent fraction of O exchange between NO_2^- and H_2O is hypothesized to be the result of the time it took for the samples to freeze and thereby slowing the exchange to a negligible rate and/or exchange that might have occurred when samples thawed.

Our samples were analyzed between 3 and 20 days of collection and were corrected assuming an O isotopic exchange of $2.7 \pm 2\%$ with water. The degree of uncertainty in the amount of $\delta^{18}\text{O}$ exchange ($\pm 2\%$) adds an uncertainty in our reported $\delta^{18}\text{O}(\text{NO}_2)$ of about 1.5‰. Therefore, the uncertainty in our $\delta^{18}\text{O}(\text{NO}_2)$ measurements is reported as $\pm 2.1‰$, which is the propagated error of our raw $\delta^{18}\text{O}(\text{NO}_2^-)$ measurement uncertainty and the uncertainty in $\delta^{18}\text{O}$ resulting from NO_2^- exchange with water.

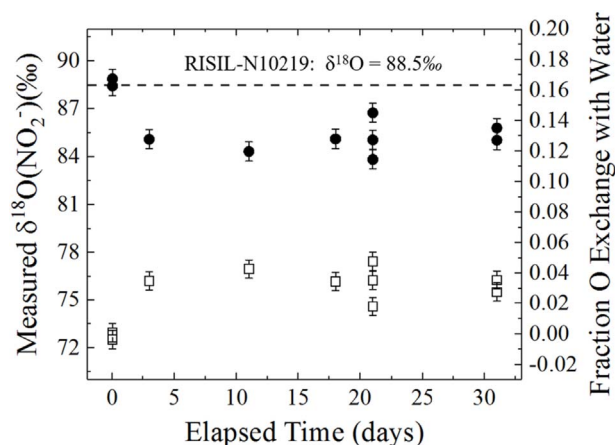


Fig. 3. Impacts of $\delta^{18}\text{O}$ exchange between NO_2^- and H_2O ($\delta^{18}\text{O} = -8‰$) contained within the KOH/guaiacol elutant as a function of time contained within solution before isotopic analysis. The black circles represent the measured $\delta^{18}\text{O}(\text{NO}_2^-)$ (primary y-axis) and the open squares represent the estimated fraction of O exchange between NO_2^- and water (secondary y-axis).

3. Results

3.1. Measured $[\text{NO}_x]$ and $f(\text{NO}_2)$

Daytime $[\text{NO}_x]$ exhibited an early morning increase between 6 and 10 a.m. that reached an average high of 7.1 ± 4.1 ppb_v around 8:00 a.m. (Fig. 4). After this morning peak, $[\text{NO}_x]$ steadily decreased throughout the day to a baseline $[\text{NO}_x]$ of approximately 2.5 ± 0.4 ppb_v (Fig. 4). A smaller NO_x peak near 5 p.m. is observed on some of the collection days during the workdays (Monday through Friday); however, this afternoon peak is not obvious in the 1 h averaged $[\text{NO}_x]$ measurements that spans the entire collection period from July 7 to August 4, 2016. It is important to note that the volume of traffic is much lower during the summertime than during the school year (September–May). A diurnal cycle in $f(\text{NO}_2)$, i.e. NO_2/NO_x , is also observed with daytime values averaging 0.82 ± 0.04 and nighttime values averaging 0.91 ± 0.004 (Fig. 4). Additionally, $f(\text{NO}_2)$ values were observed to be lowest when $[\text{NO}_x]$ concentrations were the highest.

3.2. NO_2 isotope composition

A summary of the collected NO_2 samples is reported in the Supporting Information (Table S1) that includes the sampling start and end times, the average $[\text{NO}_x]$ and $f(\text{NO}_2)$ during each collection period measured from the Thermo 42C NO_x analyzer, meteorology data including temperature, relative humidity and any meteorological events that occurred (e.g. fog and rain) (assessed via wunderground.com), collection yields, and measured $\delta^{18}\text{O}$, and $\delta^{15}\text{N}$. As a quality control of the data, we only use collected samples in which collection yields were within 15% of quantitative collection. This cutoff point is chosen based on the propagated error of quantitative collection of approximately 15% that includes the analytical error in flow rate, $[\text{NO}_2^-]$ determination, and the Thermo 42C NO_x analyzer. Out of 32 samples 23 were found to be within the propagated error limits of quantitative collection. The data that was found to result in incomplete collection occurred mostly during fog events, rain, and/or under high relative humidity conditions and probably represents a collection artifact resulting from NO_2 reactions on the wetted filter, NO_2 loss on the tubing inlet, or incomplete capture of NO_2 using the denuder under high relative humidity conditions. Interestingly, the fog and rain events that resulted in a lower than expected collection yield, had relatively elevated $\delta^{15}\text{N}(\text{NO}_2)$ values ranging from -4.2 – $7.8‰$ and averaging $(-0.1 \pm 4.2‰)$ (Table S1), and while we cannot rule out the possibility of collection artifacts during these sampling periods, these $\delta^{15}\text{N}(\text{NO}_2)$ values may

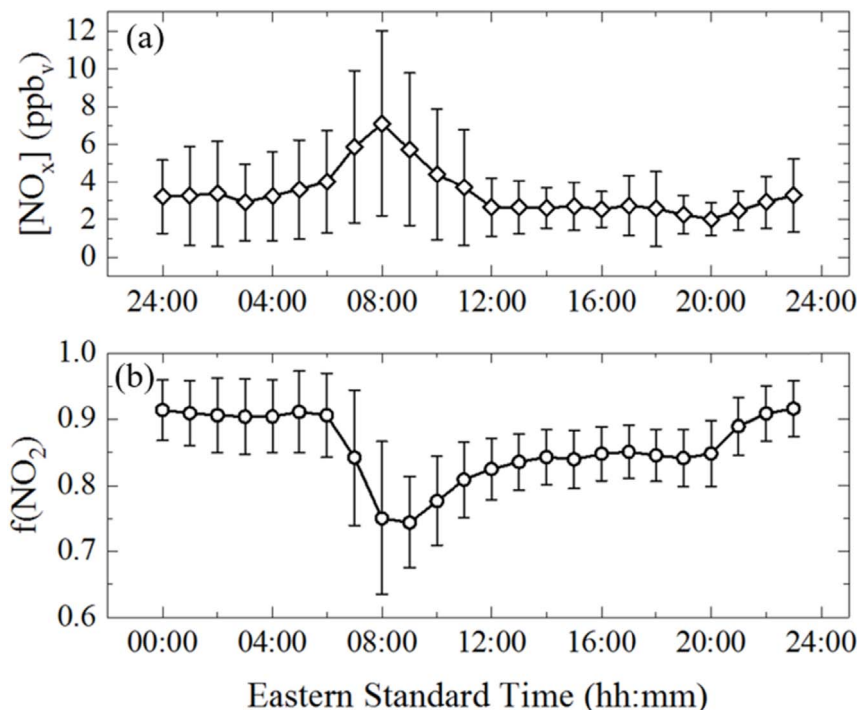


Fig. 4. Averaged diurnal variations in [NO_x] (a) and $f(\text{NO}_2)$ (b) at our sampling location during the collection period of July 7 to August 4, 2016. Diamonds represent averages for each hour taken from measurements at 30 s intervals each day and the gray lines represent $\pm 1\sigma$ for each hour.

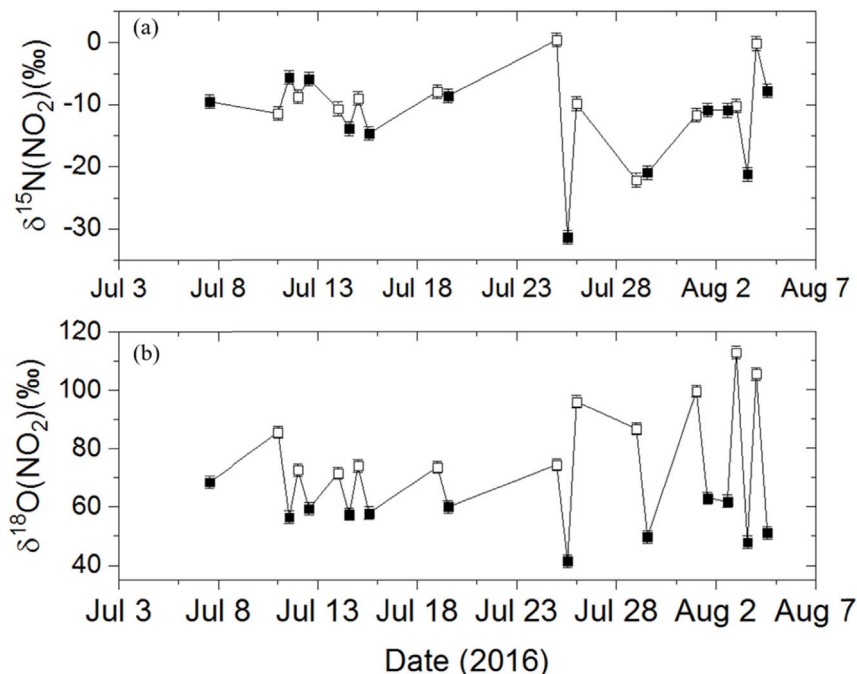


Fig. 5. Measured (a) $\delta^{15}\text{N}(\text{NO}_2)$ and (b) $\delta^{18}\text{O}(\text{NO}_2)$ of *in situ* NO_x collected from July 7, 2016 to August 5, 2016 during the daytime (open squares) and nighttime (black squares).

also be influenced by wet scavenging of NO₂ (e.g. Yoo et al., 2014), which may preferentially remove ¹⁴NO₂ leaving the collected NO₂ with higher $\delta^{15}\text{N}$ values. The measured $\delta^{15}\text{N}$ and $\delta^{18}\text{O}$ of the quality controlled data ($\pm 15\%$ within quantitative NO₂ collection) are displayed in Fig. 5.

3.2.1. Diurnal changes in $\delta^{15}\text{N}(\text{NO}_2)$ values

The measured $\delta^{15}\text{N}(\text{NO}_2)$ values (Fig. 5) had large variations that ranged from -31.4 to 0.4% and averaged $-11.4 \pm 6.9\%$ ($n = 23$). This $\delta^{15}\text{N}(\text{NO}_2)$ range is wider than the -9.0 to -3.6% range

previously reported in an urban location (Dahal and Hastings, 2016), but near the reported range of -24.6% to 7.3% measured from a roadside transect (Redling et al., 2013). The average $\delta^{15}\text{N}(\text{NO}_2)$ value is close to the $\delta^{15}\text{N}(\text{NO}_x)$ value of approximately -9% predicted by isotope mass-balance for the West Lafayette region during the July to August period (Walters et al., 2015b). Samples collected during the daytime and nighttime had an average $\delta^{15}\text{N}(\text{NO}_2)$ of $-9.2 \pm 5.7\%$ ($n = 11$) and $-13.4 \pm 7.3\%$ ($n = 12$), respectively, indicating that on average $\delta^{15}\text{N}(\text{NO}_2)$ is slightly higher during the daytime than during the nighttime. However, the difference in the daytime and nighttime

Table 1
Nighttime measured $\delta^{15}\text{N}(\text{NO}_2)$, calculated $\delta^{15}\text{N}(\text{NO}_2)$ shift, and estimated $\delta^{15}\text{N}(\text{NO}_x)$.

Collection Start	Collection End	Average $f(\text{NO}_2)$	$\delta^{15}\text{N}(\text{NO}_2)$ (‰) (Measured)	Calculated $\delta^{15}\text{N}(\text{NO}_2)$ Shift (‰) ^a	$\delta^{15}\text{N}(\text{NO}_x)$ (‰) ^b
7/7/2016 21:30	7/8/2016 5:30	0.901	-9.5	2.1	-11.6
7/11/2016 21:30	7/12/2016 5:30	0.939	-5.6	1.3	-6.9
7/12/2016 21:30	7/13/2016 5:30	0.935	-5.9	1.4	-7.2
7/14/2016 21:30	7/15/2016 5:30	0.881	-13.9	2.5	-16.4
7/15/2016 21:30	7/16/2016 5:30	0.894	-14.6	2.2	-16.8
7/19/2016 21:30	7/20/2016 5:30	0.932	-8.6	1.4	-10.0
7/25/2016 21:30	7/26/2016 5:30	0.891	-31.4	2.3	-33.8
7/29/2016 21:30	7/30/2016 5:30	0.929	-21.0	1.5	-22.5
8/1/2016 21:30	8/2/2016 5:30	0.917	-10.9	1.7	-12.6
8/2/2016 21:30	8/3/2016 5:30	0.938	-10.9	1.3	-12.2
8/3/2016 21:30	8/4/2016 5:30	0.909	-21.3	1.9	-23.2
8/4/2016 21:30	8/5/2016 5:30	0.891	-7.8	2.3	-10.1

^a $\delta^{15}\text{N}(\text{NO}_2)$ shift was calculated according to Eq. (1).

^b $\delta^{15}\text{N}(\text{NO}_x) = [\delta^{15}\text{N}(\text{NO}_2) \text{ (Measured)}] - [\delta^{15}\text{N}(\text{NO}_2) \text{ Shift}]$.

means are not statistically significant (two-sided t -test $p > 0.05$).

3.2.2. Diurnal changes in $\delta^{18}\text{O}(\text{NO}_2)$ values

Large variations were also observed in $\delta^{18}\text{O}(\text{NO}_2)$ values (Fig. 5) that ranged from 41.5 to 112.7‰ and averaged $70.7 \pm 18.7\%$ ($n = 23$). The standard deviation in $\delta^{18}\text{O}(\text{NO}_2)$ is significantly reduced when comparing daytime to nighttime collections. During the daytime, $\delta^{18}\text{O}(\text{NO}_2)$ averaged $86.5 \pm 14.1\%$ ($n = 11$), while during the nighttime, $\delta^{18}\text{O}(\text{NO}_2)$ averaged $56.3 \pm 7.1\%$ ($n = 12$). The daytime and nighttime means are statistically significantly different (two-side t -test $p < 0.05$). These $\delta^{18}\text{O}(\text{NO}_2)$ values are both larger and more variable than recently reported $\delta^{18}\text{O}(\text{NO}_2)$ values of $50.5 \pm 3.2\%$ and $47.4 \pm 1.2\%$ for NO_2 collected using Ogawa diffusion samplers at an urban location during the summer and winter, respectively (Dahal and Hastings, 2016). Additionally, our $\delta^{18}\text{O}(\text{NO}_2)$ values are much larger than reported values of $-12.6 \pm 3.1\%$ and $-2.0 \pm 5.0\%$ of NO_2 collected using Ogawa diffusion samplers placed inside and outside of a road tunnel (Felix and Elliott, 2014).

4. Discussion

4.1. Measured $[\text{NO}_x]$ and $f(\text{NO}_2)$

The large influence of traffic NO_x emission is observable in the early morning rush-hour $[\text{NO}_x]$ peak that averaged 7.1 ± 4.1 ppb_v around 8:00 a.m. (Fig. 4). This early morning NO_x emission spike is typical of urban areas (Boersma et al., 2009; Gao, 2007; Murphy et al., 2006). An afternoon rush-hour peak in $[\text{NO}_x]$ is not observed in Fig. 4. This is likely an atmospheric dilution effect caused by an increased boundary layer height and the breakdown of the early morning nocturnal inversion layer (Gaur et al., 2014). Higher afternoon oxidant concentrations that quickly converts NO_x to atmospheric nitrate may also be a factor in keeping afternoon NO_x concentrations low relative to the morning (Boersma et al., 2009). During the nighttime, $[\text{NO}_x]$ concentrations remain relatively steady, between 3 and 5 ppb_v (Fig. 4), due to the decreased boundary layer height and the titration of O_3 by NO (Nishanth et al., 2012).

The emission of NO_x and its photochemical cycling plays a significant role on the observed diurnal cycle in $f(\text{NO}_2)$ (Fig. 4). Mobile emission of NO_x is primarily in the form of NO resulting in a decrease in $f(\text{NO}_2)$ during the early morning rush-hour NO_x spike (Fig. 4). In addition, the photolysis of NO_2 results in a lower $f(\text{NO}_2)$ value during the daytime relative to the nighttime when photolysis of NO_2 ceases and nighttime oxidation of NO by O_3 pushes nighttime NO_x towards NO_2 , which is evident by the nighttime $f(\text{NO}_2)$ close to 1 (Fig. 4).

4.2. $\delta^{15}\text{N}(\text{NO}_2)$

The observed $\delta^{15}\text{N}(\text{NO}_2)$ may reflect NO_x emission sources with characteristic $\delta^{15}\text{N}$ values (e.g. Felix et al., 2012; Fibiger et al., 2014; Miller et al., 2017; Walters et al., 2015a, 2015b), isotope effects associated with the partitioning of $\delta^{15}\text{N}$ between NO and NO_2 (Walters et al., 2016; Walters and Michalski, 2015), post NO_2 oxidation reactions (Freyer, 1991; Walters and Michalski, 2015), and/or a combination of these effects. Therefore, to understand the drivers behind the observed variability in $\delta^{15}\text{N}(\text{NO}_2)$ we need to systematically evaluate these effects.

4.2.1. $\delta^{15}\text{N}(\text{NO}_2)$ isotope effect influence

During the nighttime, nearly all NO_x exists as NO_2 (Fig. 4), as we found nighttime $f(\text{NO}_2)$ to average 0.913 for the collected samples. Therefore, $\delta^{15}\text{N}(\text{NO}_2)$ values should be close to $\delta^{15}\text{N}(\text{NO}_x)$, but not exactly equal to one another since $f(\text{NO}_2) \neq 1$; Walters et al., 2016). We estimate the possible $\delta^{15}\text{N}$ effect on NO_2 relative to NO_x assuming NO_x isotope exchange is the primary driver of $\delta^{15}\text{N}$ partitioning between NO and NO_2 during the nighttime (Freyer et al., 1993; Walters et al., 2016) using Eq. (1):

$$\delta^{15}\text{N}(\text{NO}_2)(\text{‰}) = 1000 \left[\frac{(\alpha_{\text{NO}_2/\text{NO}} - 1)(1 - f_{\text{NO}_2})}{(1 - f_{\text{NO}_2}) + (\alpha_{\text{NO}_2/\text{NO}} f_{\text{NO}_2})} \right] \quad (1)$$

Where $\alpha_{\text{NO}_2/\text{NO}}$ is the N isotopic fractionation factor between NO_2 and NO during the nighttime, which was previously reported to be 1.0216 based on field measurements (Freyer et al., 1993). Using Eq. (1), we have estimated the possible $\delta^{15}\text{N}$ shift in NO_2 relative to NO_x to range between 1.3 and 2.5‰, indicating that $\delta^{15}\text{N}(\text{NO}_2)$ may be slightly higher relative to the total $\delta^{15}\text{N}(\text{NO}_x)$ during the nighttime under our sampling conditions (Table 1). Future NO_x speciated $\delta^{15}\text{N}$ measurements are necessary to confirm the predicted $\delta^{15}\text{N}$ increase in NO_2 relative to NO under nighttime conditions, and this will be the focus for future research.

Nighttime post- NO_2 oxidation reactions would likely occur via nighttime NO_2 , NO_3 , and N_2O_5 equilibration and subsequent hydrolysis of N_2O_5 to form HNO_3 (Calvert et al., 1985). The nighttime lifetime of NO_2 can be approximated based on its reaction with O_3 to form NO_3 . We estimate an approximate chemical lifetime (τ) of 21.0 h assuming nighttime $[\text{O}_3]$ of 15 ppb_v (taken from nighttime measured $[\text{O}_3]$ during July 2016 at Flora, IN, which is approximately 40 km east of the sampling site; <http://www.in.gov/idem/airquality>) and a reaction rate at 298 K, of $3.52 \times 10^{-17} \text{ cm}^3 \text{ molecules}^{-1} \text{ s}^{-1}$ ($k_{\text{NO}_2+\text{O}_3}$; Atkinson et al., 2004) and calculated according to Eq. (2):

$$\tau = \frac{1}{k_{\text{NO}_2+\text{O}_3} [\text{O}_3]} \quad (2)$$

This nighttime NO₂ lifetime is relatively long especially considering the lifetime of NO₃ resulting in the back formation of NO₂, which may occur through NO₃ reaction with NO. We estimate a nighttime NO₃ lifetime of 5.1 s, which is calculated assuming an observed average night NO concentration of approximately 0.3 ppb_v and a reaction rate at 298 K of $2.60 \times 10^{-11} \text{ cm}^3 \cdot \text{molecules}^{-1} \text{ s}^{-1}$ (Atkinson et al., 2004) (Eq. (3)):

$$\tau = \frac{1}{k_{\text{NO}_3+\text{NO}}[\text{NO}]} \quad (3)$$

Therefore, it is approximately assumed that nighttime $\delta^{15}\text{N}(\text{NO}_2)$ should reflect a mixture of local NO_x sources and possibly NO_x isotope exchange, as post-NO₂ oxidation reactions should have a minimal influence on the NO₂ loss under ambient nighttime conditions.

Daytime $\delta^{15}\text{N}(\text{NO}_2)$ is more complicated to predict than nighttime $\delta^{15}\text{N}(\text{NO}_2)$ because the photochemical reactions involving NO_x may lead to significant $\delta^{15}\text{N}$ partitioning between NO and NO₂ (Freyer et al., 1993; Walters et al., 2016). The average of $f(\text{NO}_2)$ during our daytime collection periods was 0.745, indicating that partitioning of $\delta^{15}\text{N}$ between NO and NO₂ could be significant; however, under summertime conditions at our sampling site, (i.e. $[\text{NO}_x] \ll [\text{O}_3]$) the photochemical reactions should destroy NO_x isotopic equilibrium (Freyer et al., 1993). We estimate NO_x photochemical cycling on $\delta^{15}\text{N}(\text{NO}_2)$ assuming the partitioning of ^{15}N between NO and NO₂ to be influenced by NO oxidation, NO₂ photolysis, and NO \leftrightarrow NO₂ isotopic exchange (Walters et al., 2016). Currently, we know the experimental fractionation factor for NO \leftrightarrow NO₂ isotopic exchange ($^{15}\alpha_{\text{NO}_2/\text{NO}} = 1.0356 \pm 0.0015$ at 297 K; Walters et al., 2016) and an estimated fractionation factor for NO oxidation by O₃ from *ab initio* methods ($^{15}\alpha_{\text{NO}_2/\text{NO}} = 0.993$ at 298 K (Walters and Michalski, 2016b));, but the NO₂ photolysis isotope effect is unknown. For our model, we assume no isotopic fractionation associated with NO₂ photolysis. Utilizing these isotopic fractionation factors and reaction rates (Atkinson et al., 2004; Sharma et al., 1970), we have constructed a simple box model to estimate the photochemical isotope effect on $\delta^{15}\text{N}(\text{NO}_2)$ for each of our daytime sampling conditions (Table 2).

The NO_x photochemical inputs included NO_x concentrations based on the measured average NO_x for each sampling period and O₃ concentrations estimated from reported average daily measurements from Flora, IN (taken from <http://www.in.gov/idem/airquality>) and to simplify the model, it was assumed the average O₃ represents a steady-state O₃ concentration. NO₂ photolysis rates were optimized to achieve a modeled $f(\text{NO}_2)$ that was close to the average measured value. The results of this simple box model are displayed in Table 3. Overall, we see that the competing NO_x photochemical isotope effects tend to cancel out resulting in a small $\delta^{15}\text{N}(\text{NO}_2)$ shift relative to $\delta^{15}\text{N}(\text{NO}_x)$ of 0.1–2.4%. Thus, this simple model suggests that daytime NO_x

Table 2

Summary of the NO_x photochemical nitrogen isotope box model including reaction specific fractionation factors (α), reaction rates at 298 K ($k(298 \text{ K})$) and NO₂ photolysis rate (j).

Reaction	α	$k(298 \text{ K})^a$	$j(\text{NO}_2)^b$
NO Oxidation			
$^{14}\text{NO} + \text{O}_3 \rightarrow ^{14}\text{NO}_2 + \text{O}_2$	1	1.73	–
$^{15}\text{NO} + \text{O}_3 \rightarrow ^{15}\text{NO}_2 + \text{O}_2$	0.993	1.72	–
NO_x Isotope Exchange			
$^{14}\text{NO} + ^{15}\text{NO}_2 \rightarrow ^{15}\text{NO} + ^{14}\text{NO}_2$	1	8.14	–
$^{15}\text{NO} + ^{14}\text{NO}_2 \rightarrow ^{14}\text{NO} + ^{15}\text{NO}_2$	1.0356	8.43	–
NO₂ Photolysis			
$^{14}\text{NO}_2 + h\nu \rightarrow ^{14}\text{NO} + \text{O}$	1	–	optimized
$^{15}\text{NO}_2 + h\nu \rightarrow ^{15}\text{NO} + \text{O}$	1	–	optimized

^a ($10^{-14} \text{ cm}^3 \cdot \text{molecules}^{-1} \cdot \text{s}^{-1}$) from (Atkinson et al., 2004; Sharma et al., 1970).

^b $j(\text{NO}_2)$ was optimized such that model $f(\text{NO}_2) \approx$ measured average $f(\text{NO}_2)$ for each collection period.

Table 3 Summary of daytime NO_x photochemical $\delta^{15}\text{N}$ box model. Model inputs include average measured NO_x (Avg [NO]_M), O₃ concentrations (Avg [O₃]), and $j(\text{NO}_2)$ (optimized to achieve a model $f(\text{NO}_2)$ that is approximately equal to the averaged measured $f(\text{NO}_2)$) (Avg $f(\text{NO}_2)_M$). Model outputs include the estimated $\delta^{15}\text{N}(\text{NO}_2)$ shift relative to $\delta^{15}\text{N}(\text{NO}_x)$.

Collection Start	Collection End	Avg [NO _x] _M (ppb _v)	Avg [O ₃] (ppb _v) ^a	NO _x /O ₃	Model $j(\text{NO}_2)^b$	Model $f(\text{NO}_2)$	Estimated $\delta^{15}\text{N}(\text{NO}_2)$ Shift (‰)	Estimated $\delta^{15}\text{N}(\text{NO}_2)$ (‰) ^c
7/11/2016 8:30	7/11/2016 16:00	3.8	47	0.08	3.8	0.84	0.5	-11.9
7/12/2016 8:30	7/12/2016 16:00	3.4	33.6	0.10	3.4	0.80	0.9	-9.6
7/14/2016 8:40	7/14/2016 15:50	1.9	35.3	0.05	3.4	0.80	0.1	-10.8
7/15/2016 8:40	7/15/2016 15:40	2.1	31.9	0.07	4.5	0.75	0.3	-9.2
7/19/2016 9:10	7/19/2016 15:30	2.9	39.4	0.07	3.5	0.83	0.4	-8.3
7/25/2016 9:05	7/25/2016 15:40	2.3	38.8	0.06	4.2	0.80	0.2	0.2
7/26/2016 8:40	7/26/2016 15:40	5.8	35.8	0.16	7.3	0.68	2.4	-12.2
7/29/2016 8:45	7/29/2016 15:50	4.2	41	0.10	7.6	0.70	1.1	-23.3
8/1/2016 8:30	8/1/2016 15:50	5.3	37.4	0.14	10.5	0.61	2	-13.6
8/3/2016 8:50	8/3/2016 15:30	5.5	54.2	0.10	10.5	0.69	1.1	-11.3
8/4/2016 8:50	8/4/2016 15:05	7.9	51.1	0.15	10.5	0.69	2.3	-2.5

^a Average measured O₃ at Flora, IN (<http://www.in.gov/idem/airquality>) for each collection period.

^b (10^{-3} s^{-1}).

^c $\delta^{15}\text{N}(\text{NO}_2) = [\delta^{15}\text{N}(\text{NO}_2) (\text{Measured})] - [\delta^{15}\text{N}(\text{NO}_2) \text{ Shift}]$.

photochemical isotope effects at our sampling location should be small. We note the uncertainty in the NO_2 photolysis isotope effect and future work will need to determine this value. However, varying the NO_2 photolysis fractionation factor from 0.995 to 1.005 in our model resulted in a shift in the calculated $\delta^{15}\text{N}(\text{NO}_2)$ of approximately 1‰, indicating this effect to be small. We emphasize that this simple box model roughly approximates the $\delta^{15}\text{N}(\text{NO}_2)$ daytime isotope effect and future chemical kinetic modeling will need to be done to better predict this isotope effect. Additionally, future NO_x speciation and $\delta^{15}\text{N}$ measurements will be helpful in determining the conditions that may influence daytime $\delta^{15}\text{N}$ partitioning between NO and NO_2 and its temporal variability.

In addition to photochemical cycling, post- NO_2 oxidation reactions must be taken into consideration. During the daytime, NO_2 is primarily oxidized by OH leading to the formation of HNO_3 , resulting in an NO_2 chemical lifetime on the order of a few hours (Valin et al., 2013). While this is a relatively short lifetime, the reaction between NO_2 and OH is expected to have a small kinetic isotope effect of $^{15}\alpha = 0.9971$ (Freyer, 1991). Thus, we expect this reaction to have a minimal influence on $\delta^{15}\text{N}(\text{NO}_2)$, but future work should investigate post daytime NO_2 oxidation on $\delta^{15}\text{N}(\text{NO}_x)$, which will likely require experimental chamber studies and detailed chemical kinetic models.

4.2.2. $\delta^{15}\text{N}(\text{NO}_2)$ source effect

Based off our NO_x isotope predictions, isotope effects associated with NO_x atmospheric processing are expected to have a relatively minor impact on $\delta^{15}\text{N}(\text{NO}_2)$ under our sampling conditions. Therefore, the wide variability observed in $\delta^{15}\text{N}(\text{NO}_2)$ is likely driven by changing contributions from NO_x source emissions to the measured background NO_2 . Important local NO_x emission sources near our sampling site include: biogenic NO_x , fuel combustion, and traffic with $\delta^{15}\text{N}(\text{‰})$ ranges of -59.8 to -19.9 , -19.7 to -13.7 , and -9 to -2 , respectively (Felix and Elliott, 2014; Li and Wang, 2008; Miller et al., 2017; Walters et al., 2015b; Yu and Elliott, 2017). Our measured $\delta^{15}\text{N}(\text{NO}_2)$ and predicted $\delta^{15}\text{N}(\text{NO}_x)$ (Tables 1 and 3) are generally within the range of these emission sources; therefore, the variability observed in $\delta^{15}\text{N}(\text{NO}_2)$ is likely driven by changing relative contributions from these emission sources rather than chemical processing.

To gain a better understanding of the influence of changing contributions from NO_x sources at our site and their diurnal variability, we have modeled the NO_x source contribution of our calculated $\delta^{15}\text{N}(\text{NO}_x)$ using the EPA IsoSource Model that calculates all possible unique source proportions at a source increment of 1% based of isotopic mass balance (Phillips and Gregg, 2003). We use a value of -2‰ for traffic-derived NO_x , which is based on on-road mobile measurements near urban areas (Miller et al., 2017). Local fossil-fuel combustion was assumed to have a value of -17.9‰ , which is the average value ($1\sigma = \pm 1\text{‰}$) previously measured from one of the natural gas boilers (Walters et al., 2015b) and is the main contributor to NO_x emission at the utility plant. Biogenic emitted NO_x has a large variability in $\delta^{15}\text{N}(\text{NO}_x)$ ranging from -59.8 to -19.9‰ (Felix and Elliott, 2014; Li and Wang, 2008; Yu and Elliott, 2017). For the purpose of evaluating approximate relative source contribution determination we use a soil value of -53.6‰ , which was the average value found for 12 h of post-wetting soils in a previous laboratory study (Yu and Elliott, 2017). We note that the large variability in biogenic $\delta^{15}\text{N}(\text{NO}_x)$ makes it difficult to exactly quantitatively determine NO_x source contributions, but using a set $\delta^{15}\text{N}(\text{NO}_x)$ value will help us determine approximate relative changes in NO_x source emissions at our sampling site. We have restricted our mass-balance model to these three sources since they likely play the most influential role on the local NO_x emission budget and enable an approximate evaluation of relative source contributions from these sources.

Fig. 6 displays a statistical distribution of all possible combination of solutions utilizing local NO_x sources with specified $\delta^{15}\text{N}$ that match the estimated $\delta^{15}\text{N}(\text{NO}_x)$ based off mass-balance separated for both

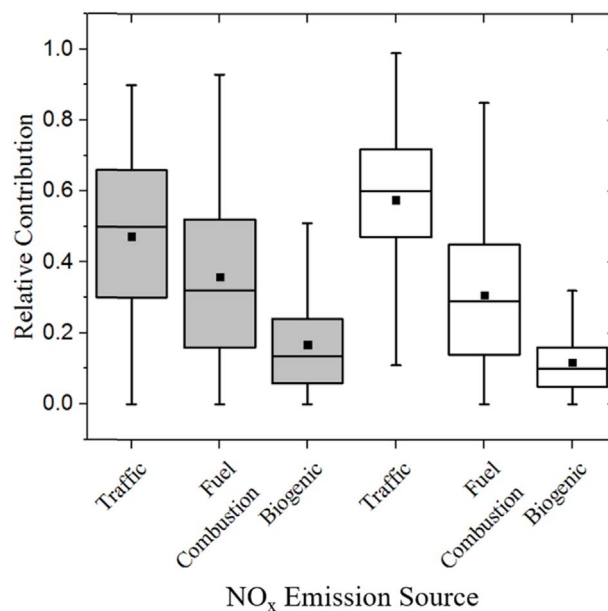


Fig. 6. Statistical distribution indicating the minimum, 25th percentile, 50th percentile, 75th percentile, maximum, and average (black square) of all feasible solutions that satisfy mass-balance between the assumed major local NO_x emission sources and estimated $\delta^{15}\text{N}(\text{NO}_x)$ based on our $\delta^{15}\text{N}(\text{NO}_2)$ measurements and accounting for possible isotope effects. The gray shading corresponds to nighttime while no shading corresponds to the daytime.

daytime and nighttime collection periods. This mass-balance analysis was conducted for each sampling period except for one daytime sample (7/25/2016; Table 3), in which the estimated $\delta^{15}\text{N}(\text{NO}_x)$ value of 0.2‰ was higher than any of the NO_x emission sources and no feasible solution could be generated. However, we note that this value is nearly within analytical measurement precision of the traffic $\delta^{15}\text{N}(\text{NO}_x)$ signature. Samples collected during the night had an average solution distribution for traffic, natural gas-fired power plant, and biogenic emissions of 0.47 ± 0.22 , 0.36 ± 0.24 , and 0.17 ± 0.14 , while samples collected during the daytime had an average solution distribution for traffic, natural gas-fired power plants, and biogenic emissions of 0.58 ± 0.19 , 0.30 ± 0.20 , and 0.11 ± 0.09 . This simple mass-balance model indicates that there may be interesting temporal variability in NO_x emission sources, as the distribution of possible feasible solutions suggest that traffic NO_x contributes more to the overall daytime NO_x emission budget, which is expected due to higher daytime traffic. Combining both day and night samples yield an average solution distribution for traffic, natural gas-fired power plant, and biogenic emissions of 0.52 ± 0.22 , 0.34 ± 0.22 , and 0.15 ± 0.13 . These estimates compare reasonably well with the estimation of these sources based on the 2011 U.S. EPA national emission inventory (NEI) for the sampling location county (Tippecanoe) of Traffic = 0.594, Fuel Combustion = 0.353, Biogenic = 0.042 [Office of Air Quality Planning and Standards (2011)]. Our slightly higher predicted biogenic contribution compared to the NEI is likely explained due to the NEI data representing yearlong NO_x emission estimates, while our estimated source contribution is based on NO_x emitted during the summer, in which biogenic emissions likely play a more influential role to the local NO_x emission budget. However, we note that our mixing system is extremely simplified, and there may be other contributing NO_x emission sources at our sampling site that are not taken into account in our model.

It is important to point out that this mass-balance model is an approximation with the goal to understand the drivers of $\delta^{15}\text{N}(\text{NO}_2)$ variability in ambient/background air and not to exactly pinpoint the NO_x source proportions at our sampling location. However, this model does highlight the potential to use $\delta^{15}\text{N}(\text{NO}_x)$ to evaluate NO_x source contributions in a well-mixed area to evaluate spatial and temporal

changes. To quantitatively use this tool, we need to have a better characterization of environmental $\delta^{15}\text{N}(\text{NO}_x)$ source values and will also need to collect $\delta^{15}\text{N}(\text{NO}_x)$ from ambient air as opposed to $\delta^{15}\text{N}(\text{NO}_2)$ as conducted in this study. This is because we are still somewhat uncertain as to how NO_x processing may impact $\delta^{15}\text{N}(\text{NO}_2)$ relative to $\delta^{15}\text{N}(\text{NO}_x)$, although our calculations indicate it to be relatively small at our sampling site. Now that we have a model that may be useful to predict the $\delta^{15}\text{N}$ partitioning between NO and NO_2 , we need to validate it using simultaneous NO and NO_2 collection for $\delta^{15}\text{N}$ analysis, which will be the subject for future research.

4.3. $\delta^{18}\text{O}(\text{NO}_2)$

4.3.1. Daytime $\delta^{18}\text{O}(\text{NO}_2)$

Daytime NO_2 was highly enriched in ^{18}O , with an average $\delta^{18}\text{O}(\text{NO}_2)$ value of $86.5 \pm 14.1\text{‰}$ ($n = 11$) (Fig. 5). During the daytime, $\delta^{18}\text{O}(\text{NO}_2)$ values are expected to reflect the oxidants responsible for the conversion of NO to NO_2 , as the photochemical cycling of NO_x is rapid and should quickly erase any $\delta^{18}\text{O}(\text{NO}_x)$ source signatures. For an urban area, O_3 should dominate the conversion of NO to NO_2 (R1). Thus, $\delta^{18}\text{O}(\text{NO}_2)$ values should reflect NO_x photochemical equilibrium with O_3 that has a high $\delta^{18}\text{O}$ value (Alexander et al., 2009; Michalski et al., 2003; Vicars and Savarino, 2014). Previously, tropospheric O_3 has been reported to have elevated $\delta^{18}\text{O}(\text{O}_3)$ values ranging from 95 to 130‰ (Johnston and Thiemens, 1997; Krankowsky et al., 1995; Vicars and Savarino, 2014), and a prior experimental investigation found that the photochemical cycling of $\text{NO-O}_2\text{-O}_3\text{-NO}_2$ to result in $\delta^{18}\text{O}(\text{NO}_2)$ of 117‰ (Michalski et al., 2014). This experimental value is near our highest measured daytime $\delta^{18}\text{O}(\text{NO}_2)$ value of 112.7‰ (Fig. 7). However, there was large variability observed in daytime $\delta^{18}\text{O}(\text{NO}_2)$ that spanned 41.2‰ across the collection periods with values as low as 71.5‰, which may not be explained by NO_x isotopic photochemical equilibrium with tropospheric O_3 .

NO may also be oxidized by peroxy radicals and this may be reflected in the $\delta^{18}\text{O}(\text{NO}_2)$. Peroxy radicals are estimated to have an oxygen isotopic composition that reflects tropospheric O_2 (Michalski et al., 2012) that is approximately 23‰ (Kroopnick and Craig, 1972). Assuming no isotope effect during the $\text{NO} + \text{RO}_2$ (or HO_2) reaction, the O transferred from RO_2 (or HO_2) to NO_2 can be approximated to be the $\delta^{18}\text{O}(\text{RO}_2\text{(or HO}_2)) \approx 23\text{‰}$. Thus, the lower daytime $\delta^{18}\text{O}(\text{NO}_2)$ values may be the result of NO oxidation by peroxy radicals. An isotope mass-balance model can be used to estimate the NO oxidation branching ratio (x):

$$\delta^{18}\text{O}(\text{NO}_2) = x \times (\delta^{18}\text{O}(\text{O}_3)) + (1 - x) \times (\delta^{18}\text{O}(\text{ROO}\cdot\text{orHOO}\cdot)) \quad (4)$$

Where $\delta^{18}\text{O}(\text{NO}_2)$ is the observed NO_2 $\delta^{18}\text{O}$ values that is produced by fractions of oxygen derived from O_3 (117‰) and peroxy radicals (23‰). Using these oxidant end-member $\delta^{18}\text{O}$ values, we estimate the daytime branching ratio of NO oxidation by O_3 to be 0.68 ± 0.15 , signifying that O_3 was generally the dominate daytime oxidant at our sampling location as expected. However, NO oxidation through peroxy radicals seems to have played a significant role and reached a branching ratio as high as 0.48 during our sampling periods (Fig. 7). This is important since NO oxidation through peroxy radicals occurs without the loss of O_3 providing a pathway for the buildup of tropospheric O_3 . Thus, the isotopic composition of daytime NO_2 may provide a useful way to assess $\text{VOC-NO}_x\text{-O}_3$ chemistry, which is a fundamental underpinning of atmospheric chemistry modeling.

To assess whether the estimated NO branching ratio based on $\delta^{18}\text{O-NO}_2$ is reasonable, we have compared our results to a simulation from the RACM model (Stockwell et al., 1997) that included photolysis parameters at our sampling site in July (Madronich, 1987). We chose to run the RACM model with initial conditions corresponding to rural summer surface case 8 and 9 as described in (Stockwell et al., 1997). Briefly, $[\text{NO}_x]$ is set to 5 ppb_v, which is relatively close to the observed daytime $[\text{NO}_x]$ (Fig. 4), and the concentration of nonmethane organic carbon (NMOC) is set to 33 ppb_v and 100 ppb_v for case 8 and case 9, respectively. While these conditions are not the exact conditions of our sampling site, it should provide an approximate expectation of the NO oxidation branching ratio for comparison to the branching ratio derived from our $\delta^{18}\text{O}$ results. A two-day simulation was run and the branching ratio of NO oxidation by O_3 was calculated to be of 0.8516 ± 0.019 ($\bar{X} \pm \sigma$) and 0.7599 ± 0.020 , under the initial condition of low and high concentrations of organic compound, respectively. These branching ratios compare well with our estimated value of 0.68 ± 0.15 based on daytime $\delta^{18}\text{O}(\text{NO}_2)$ measurements. The modeling results support our hypothesis that the oxidants responsible for the oxidation of NO can be roughly approximated using $\delta^{18}\text{O}(\text{NO}_2)$, which has important implications for evaluating the impact of NO_x emissions on oxidation chemistry.

4.3.2. Nighttime $\delta^{18}\text{O}(\text{NO}_2)$

Nighttime NO_2 was found to have low $\delta^{18}\text{O}$ values relative to the daytime, averaging $56.3 \pm 7.1\text{‰}$. This is likely the result of the absence of NO_x photochemical cycling during the night, limiting isotopic equilibrium between NO_x and its oxidants. We hypothesize that NO_2 produced during the night should reflect the mass-balance between $\delta^{18}\text{O}$ of the emitted nighttime NO and the $\delta^{18}\text{O}$ of the O atom transferred from the responsible oxidant ($\delta^{18}\text{O}(\text{O}_{\text{trans}})$):

$$\delta^{18}\text{O}(\text{NO}_{2\text{night}}) = \frac{1}{2}(\delta^{18}\text{O}(\text{NO}_{\text{source}})) + \frac{1}{2}(\delta^{18}\text{O}(\text{O}_{\text{trans}})) \quad (5)$$

Thus, a portion of the oxygen in nighttime NO_2 should be from the NO source that likely has a relatively lower $\delta^{18}\text{O}$ than does the main NO oxidant, O_3 , resulting in a lower nighttime $\delta^{18}\text{O}(\text{NO}_2)$ during the night relative to the day. It is important to note that NO_2 collected during the nighttime will not entirely reflect the mass-balance between $\delta^{18}\text{O}(\text{NO})$ and $\delta^{18}\text{O}(\text{O}_{\text{trans}})$ (Eq. (5)). This is because there is residual daytime NO_2 , which reached photochemical equilibrium with atmospheric oxidants, that is also collected during the nighttime. The daytime lifetime of NO_2 can be estimated to be approximately 6.8 h assuming that OH is the main sink ($k(\text{NO}_2 + \cdot\text{OH})_{298\text{K}} = 4.1 \times 10^{-11} \text{ cm}^3 \text{ molecules}^{-1} \text{ s}^{-1}$ (Atkinson et al., 2004); $[\text{OH}] = 1 \times 10^{-6} \text{ molecules cm}^{-3}$). Thus, there will still be photochemically cycled NO_2 present during our nighttime collection. Due to this interference, it is difficult to estimate the $\delta^{18}\text{O}(\text{NO}_{\text{source}})$ values using back-calculation of Eq. (5). However, our results indicate that $\delta^{18}\text{O}(\text{NO}_{\text{source}})$ should have a relatively lower $\delta^{18}\text{O}$ value compared to the NO oxidants. Additionally, future work should aim to quantify $\delta^{18}\text{O}(\text{NO}_x)$ of emission sources since this likely plays a role in

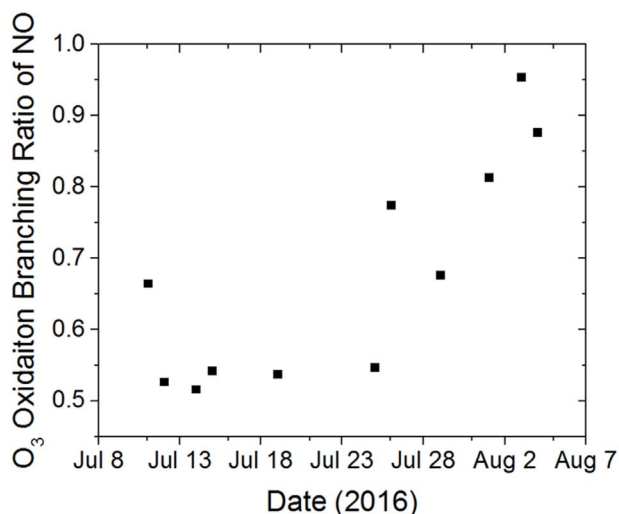


Fig. 7. Estimated NO oxidation branching ratio between O_3 (red) and $\text{ROO}\cdot$ (black) calculated from Eq. (4).

observed $\delta^{18}\text{O}(\text{NO}_2)$ values during the nighttime.

5. Conclusion

Diurnal variability in $\delta^{15}\text{N}$ and $\delta^{18}\text{O}$ of ambient NO_2 was assessed at a small Midwestern city. Overall, we predict that variability in $\delta^{15}\text{N}$ (NO_2) is largely driven by changing contributions from local NO_x source emissions as predicted isotope effects under the sampling conditions are expected to be small $< 2.5\%$. A statistical mass-balance model indicates that there may be interesting temporal variabilities in NO_x emission sources with higher traffic contribution during the daytime. Results also indicate that biogenic emissions during the summer might be a significant contributor to local NO_x emission budgets estimated to represent $15 \pm 13\%$ at the sampling site. The relatively minor partitioning between NO and NO_2 predicted at our sampling site indicates that during the summer under conditions of $[\text{NO}_x] \ll [\text{O}_3]$, $\delta^{15}\text{N}$ should be approximately conserved as NO_x is transformed into atmospheric nitrate, but future chamber studies are necessary to evaluate isotope effects associated with post NO_2 oxidation. Variability in $\delta^{18}\text{O}(\text{NO}_2)$ is driven by the photochemical cycling of NO_x , in which NO reactions with O_3 produce an elevated $\delta^{18}\text{O}$ value. During the nighttime, $\delta^{18}\text{O}$ (NO_2) values are lower due to $\delta^{18}\text{O}$ contributions from NO_x emission sources with hypothesized lower $\delta^{18}\text{O}$ values than atmospheric oxidants and due to the absence of NO_x photochemical cycling.

Future work should aim toward fine-tuning our method to develop collection techniques that can be used to characterize $\delta^{15}\text{N}$, $\delta^{18}\text{O}$, and $\Delta^{17}\text{O}$ of NO_2 under optimized conditions and at higher time resolution. This could be achieved using a more sophisticated denuder setup utilizing annular or honeycomb denuder geometries. Future speciated NO_x $\delta^{15}\text{N}$ measurements are needed to fully understand the atmospheric processes that dictate the $\delta^{15}\text{N}$ partitioning between NO and NO_2 under environmental conditions, and this will be the subject for future research. Additionally, the results suggest the potential to use $\delta^{15}\text{N}(\text{NO}_x)$ to evaluate NO_x source contributions under ambient conditions, but in order to quantitatively use this tool, future work must better characterize environmental $\delta^{15}\text{N}(\text{NO}_x)$ source signatures, as well to better quantify the isotope effects during NO_x photochemical cycling after its emission.

Acknowledgements

One of the authors (W.W.W.) was a National Science Foundation Graduate Research Fellow during the study. We would like to thank the Purdue Climate Change Research Center (PCCRC) graduate fellowship program and the Purdue Bilsland Dissertation Fellowship for supporting this work.

Appendix A. Supplementary data

Supplementary data related to this article can be found at <http://dx.doi.org/10.1016/j.atmosenv.2018.01.047>.

References

- Alexander, B., Hastings, M.G., Allman, D.J., Dachs, J., Thornton, J.A., Kunasek, S.A., 2009. Quantifying atmospheric nitrate formation pathways based on a global model of the oxygen isotopic composition ($\Delta^{17}\text{O}$) of atmospheric nitrate. *Atmos. Chem. Phys.* 9 (14), 5043–5056.
- Ali, Z., Thomas, C.L.P., Alder, J.F., 1989. Denuder tubes for sampling of gaseous species. A review. *Analyst* 114 (7), 759–769.
- Ammann, M., Siegwolf, R., Pichlmayer, F., Suter, M., Saurer, M., Brunold, C., 1999. Estimating the uptake of traffic-derived NO_2 from ^{15}N abundance in Norway spruce needles. *Oecologia* 118 (2), 124–131.
- Ammann, M., Rössler, E., Streckowski, R., George, C., 2005. Nitrogen dioxide multiphase chemistry: uptake kinetics on aqueous solutions containing phenolic compounds. *7* (12), 2513–2518.
- Atkinson, R., 2000. Atmospheric chemistry of VOCs and NO_x . *Atmos. Environ.* 34 (12), 2063–2101.
- Atkinson, R., Arey, J., 2003. Gas-phase tropospheric chemistry of biogenic volatile organic compounds: a review. *Atmos. Environ.* 37, 197–219.
- Atkinson, R., Baulch, D.L., Cox, R.A., Crowley, J.N., Hampson, R.F., Hynes, R.G., Troe, J., 2004. Evaluated kinetic and photochemical data for atmospheric chemistry: volume I-gas phase reactions of O_x , HO_x , NO_x and SO_x species. *Atmos. Chem. Phys.* 4 (6), 1461–1738.
- Boersma, K.F., Jacob, D.J., Trainic, M., Rudich, Y., DeSmedt, I., Dirksen, R., Eskes, H.J., 2009. Validation of urban NO_2 concentrations and their diurnal and seasonal variations observed from the SCIAMACHY and OMI sensors using in situ surface measurements in Israeli cities. *Atmos. Chem. Phys.* 9 (12), 3867–3879.
- Böhlke, J.K., Smith, R.L., Hannon, J.E., 2007. Isotopic analysis of N and O in nitrite and nitrate by sequential selective bacterial reduction to N_2O . *Anal. Chem.* 79 (15), 5888–5895.
- Buttini, P., Di Palo, V., Possanzini, M., 1987. Coupling of denuder and ion chromatographic techniques for NO_2 trace level determination in air. *Sci. Total Environ.* 61, 59–72.
- Calvert, J.G., Lazrus, A., Kok, G.L., Heikes, B.G., Walega, J.G., Lind, J., Cantrell, C.A., 1985. Chemical mechanisms of acid generation in the troposphere. *Nature* 317 (6032), 27–35.
- Casciotti, K.L., Böhlke, J.K., McIlvin, M.R., Mroczkowski, S.J., Hannon, J.E., 2007. Oxygen isotopes in nitrite: analysis, calibration, and equilibration. *Anal. Chem.* 79 (6), 2427–2436.
- Crutzen, P.J., 1973. Gas-phase Nitrogen and Methane Chemistry in the Atmosphere. D. Reidel Publishing Company, Dordrecht, Holland.
- Crutzen, P.J., 1979. The role of NO and NO_2 in the chemistry of the troposphere and stratosphere. *Annu. Rev. Earth Planet Sci.* 7, 443–472.
- Dahal, B., Hastings, M.G., 2016. Technical considerations for the use of passive samplers to quantify the isotopic composition of NO_x and NO_2 using the denitrifier method. *Atmos. Environ.* 143, 60–66.
- Febo, A., Perrino, C., Cortiello, M., 1993. A denuder technique for the measurement of nitrous acid in urban atmospheres. *Atmos. Environ. Part A. General Topics* 27 (11), 1721–1728.
- Felix, J.D., Elliott, E.M., 2013. The agricultural history of human-nitrogen interactions as recorded in ice core $\delta^{15}\text{N}-\text{NO}_3^-$. *Geophys. Res. Lett.* 40 (8), 1642–1646.
- Felix, J.D., Elliott, E.M., 2014. Isotopic composition of passively collected nitrogen dioxide emissions: vehicle, soil and livestock source signatures. *Atmos. Environ.* 92, 359–366.
- Felix, J.D., Elliott, E.M., Shaw, S.L., 2012. Nitrogen isotopic composition of coal-fired power plant NO_x : influence of emission controls and implications for global emission inventories. *Environ. Sci. Technol.* 46 (6), 3528–3535.
- Fibiger, D.L., Hastings, M.G., Lew, A.F., Peltier, R.E., 2014. Collection of NO and NO_2 for isotopic analysis of NO_x emissions. *Anal. Chem.* 86 (24), 12115–12121.
- Freyer, H.D., 1991. Seasonal variation of $^{15}\text{N}/^{14}\text{N}$ ratios in atmospheric nitrate species. *Tellus B* 43 (1), 30–44.
- Freyer, H.D., Kley, D., Volz-Thomas, A., Kobel, K., 1993. On the interaction of isotopic exchange processes with photochemical reactions in atmospheric oxides of nitrogen. *J. Geophys. Res.* 98 (D8), 14791–14796.
- Galloway, J.N., Dentener, F.J., Capone, D.G., Boyer, E.W., Howarth, R.W., Seitzinger, S.P., Holland, E., 2004. Nitrogen cycles: past, present, and future. *Biogeochemistry* 70 (2), 153–226.
- Gao, H.O., 2007. Day of week effects on diurnal ozone/ NO_x cycles and transportation emissions in Southern California. *Transport. Res. Transport Environ.* 12 (4), 292–305.
- Gaur, A., Tripathi, S.N., Kanawade, V.P., Tare, V., Shukla, S.P., 2014. Four-year measurements of trace gases (SO_2 , NO_x , CO , and O_3) at an urban location, Kanpur, in Northern India. *J. Atmos. Chem.* 71 (4), 283–301.
- Harris, G.W., Carter, W.P., Winer, A.M., Pitts, J.N., Platt, U., Perner, D., 1982. Observations of nitrous acid in the Los Angeles atmosphere and implications for predictions of ozone-precursor relationships. *Environ. Sci. Technol.* 16 (7), 414–419.
- Hastings, M.G., Sigman, D.M., Lipschultz, F., 2003. Isotopic evidence for source changes of nitrate in rain at Bermuda. *J. Geophys. Res.: Atmosphere* 108 (D24).
- Heaton, T.H.E., 1987. $^{15}\text{N}/^{14}\text{N}$ ratios of nitrate and ammonium in rain at Pretoria, South Africa. *Atmos. Environ.* 21 (4), 843–852.
- Heaton, T.H.E., 1990. $^{15}\text{N}/^{14}\text{N}$ ratios of NO_x from vehicle engines and coal-fired power stations. *Tellus B* 42 (3), 304–307.
- Hoering, T., 1957. The isotopic composition of the ammonia and the nitrate ion in rain. *Geochem. Cosmochim. Acta* 12 (1–2), 97–102.
- Jaeglé, L., Steinberger, L., Martin, R.V., Chance, K., 2005. Global partitioning of NO_x sources using satellite observations: relative roles of fossil fuel combustion, biomass burning and soil emissions. *Faraday Discussions* 130, 407–423.
- Johnston, J.C., Thiemens, M.H., 1997. The isotopic composition of tropospheric ozone in three environments. *J. Geophys. Res.: Atmospheres (1984–2012)* 102 (D21), 25395–25404.
- Krankowsky, D., Bartheck, F., Klees, G.G., Mauersberger, K., Schellenbach, K., Stehr, J., 1995. Measurement of heavy isotope enrichment in tropospheric ozone. *Geophys. Res. Lett.* 22 (13), 1713–1716.
- Kroopnick, P., Craig, H., 1972. Atmospheric oxygen: isotopic composition and solubility fractionation. *Science* 175 (4017), 54–55.
- Leighton, P., 1961. Photochemistry of Air Pollution. Academic, New York.
- Li, D., Wang, X., 2008. Nitrogen isotopic signature of soil-released nitric oxide (NO) after fertilizer application. *Atmos. Environ.* 42 (19), 4747–4754.
- Logan, J.A., 1983. Nitrogen oxides in the troposphere: global and regional budgets. *J. Geophys. Res.: Oceans* 88 (C15), 10785–10807.
- Madronich, S., 1987. Photodissociation in the atmosphere: 1. Actinic flux and the effects of ground reflections and clouds. *J. Geophys. Res.: Atmosphere* 92 (D8), 9740–9752.
- Massman, W.J., 1998. A review of the molecular diffusivities of H_2O , CO_2 , CH_4 , CO , O_3 , SO_2 , NH_3 , N_2O , NO , and NO_2 in air, O_2 and N_2 near STP. *Atmos. Environ.* 32 (6), 1111–1127.

- Mauersberger, K., Lämmerzahl, P., Krankowsky, D., 2001. Stratospheric ozone isotope enrichments—revisited. *Geophys. Res. Lett.* 28 (16), 3155–3158.
- McIlvin, M.R., Altabet, M.A., 2005. Chemical conversion of nitrate and nitrite to nitrous oxide for nitrogen and oxygen isotopic analysis in freshwater and seawater. *Anal. Chem.* 77 (17), 5589–5595.
- Michalski, G., Bhattacharya, S.K., Girsch, G., 2014. NO_x cycle and the tropospheric ozone isotope anomaly: an experimental investigation. *Atmos. Chem. Phys.* 14 (10), 4935–4953.
- Michalski, G., Bhattacharya, S.K., Mase, D.F., 2012. Oxygen isotope dynamics of atmospheric nitrate and its precursor molecules. In: *Handbook of Environmental Isotope Geochemistry*. Springer, pp. 613–635.
- Michalski, G., Scott, Z., Kabling, M., Thiemens, M.H., 2003. First measurements and modeling of $\Delta 17\text{O}$ in atmospheric nitrate. *Geophys. Res. Lett.* 30 (16), 1870.
- Miller, D.J., Wojtal, P.K., Clark, S.C., Hastings, M.G., 2017. Vehicle NO_x emission plume isotopic signatures: spatial variability across the eastern United States. *J. Geophys. Res.: Atmosphere* 122 (8) 2016JD025877.
- Moore, H., 1977. The isotopic composition of ammonia, nitrogen dioxide and nitrate in the atmosphere. *Atmos. Environ.* 11 (12), 1239–1243.
- Morin, S., Savarino, J., Frey, M.M., Yan, N., Bekki, S., Bottenheim, J.W., Martins, J.M., 2008. Tracing the origin and fate of NO_x in the Arctic atmosphere using stable isotopes in nitrate. *Science* 322 (5902), 730–732.
- Murphy, J.G., Day, D.A., Cleary, P.A., Wooldridge, P.J., Cohen, R.C., 2006. Observations of the diurnal and seasonal trends in nitrogen oxides in the western Sierra Nevada. *Atmos. Chem. Phys.* 6 (12), 5321–5338.
- Nishanth, T., Kumar, M.S., Valsaraj, K.T., 2012. Variations in surface ozone and NO_x at Kannur: a tropical, coastal site in India. *J. Atmos. Chem.* 69 (2), 101–126.
- Office of Air Quality Planning and Standards, U. E. (n.d.). 2011 National emissions inventory data & documentation. Retrieved April 16, 2015, from <http://www.epa.gov/ttn/chief/net/2011inventory.html>.
- Pearce, P.J., Simkins, R.J.J., 1968. Acid strengths of some substituted picric acids. *Can. J. Chem.* 46 (2), 241–248.
- Phillips, D.L., Gregg, J.W., 2003. Source partitioning using stable isotopes: coping with too many sources. *Oecologia* 136 (2), 261–269.
- Redling, K., Elliott, E., Bain, D., Sherwell, J., 2013. Highway contributions to reactive nitrogen deposition: tracing the fate of vehicular NO_x using stable isotopes and plant biomonitors. *Biogeochemistry* 116 (1–3), 261–274.
- Reis, S., Pinder, R.W., Zhang, M., Lijie, G., Sutton, M.A., 2009. Reactive nitrogen in atmospheric emission inventories—a review. *Atmos. Chem. Phys. Discuss.* 9, 12–413.
- Riha, K.M., 2013. The Use of Stable Isotopes to Constrain the Nitrogen Cycle. Purdue University. Retrieved from <http://docs.lib.purdue.edu/dissertations/AAI3592093/>.
- Savarino, J., Morin, S., Erbland, J., Grannec, F., Patey, M.D., Vicars, W., Achterberg, E.P., 2013. Isotopic composition of atmospheric nitrate in a tropical marine boundary layer. *Proc. Natl. Acad. Sci. U.S.A.* 110 (44), 17668–17673.
- Savarino, J., Bhattacharya, S.K., Morin, S., Baroni, M., Doussin, J.-F., 2008. The NO + O₃ reaction: a triple oxygen isotope perspective on the reaction dynamics and atmospheric implications for the transfer of the ozone isotope anomaly. *J. Chem. Phys.* 128 (19) 194303.
- Sharma, H.D., Jervis, R.E., Wong, K.Y., 1970. Isotopic exchange reactions in nitrogen oxides. *J. Phys. Chem.* 74 (4), 923–933.
- Snape, C.E., Sun, C.G., Fallick, A.E., Irons, R., Haskell, J., 2003. Potential of stable nitrogen isotope ratio measurements to resolve fuel and thermal NO_x in coal combustion. *Papers of the American Chemical Society* 225 U843–U843.
- Stockwell, W.R., Kirchner, F., Kuhn, M., Seefeld, S., 1997. A new mechanism for regional atmospheric chemistry modeling. *J. Geophys. Res.: Atmosphere* 102 (D22), 25847–25879.
- Thiemens, M.H., Heidenreich, J.E., 1983. The mass-independent fractionation of oxygen: a novel isotope effect and its possible cosmochemical implications. *Science* 219 (4588), 1073–1075.
- Valin, L.C., Russell, A.R., Cohen, R.C., 2013. Variations of OH radical in an urban plume inferred from NO₂ column measurements. *Geophys. Res. Lett.* 40 (9), 1856–1860.
- Vicars, W.C., Savarino, J., 2014. Quantitative constraints on the 17 O-excess ($\Delta 17\text{O}$) signature of surface ozone: ambient measurements from 50° N to 50° S using the nitrite-coated filter technique. *Geochem. Cosmochim. Acta* 135, 270–287.
- Vicars, W.C., Bhattacharya, S.K., Erbland, J., Savarino, J., 2012. Measurement of the 17O-excess ($\Delta 17\text{O}$) of tropospheric ozone using a nitrite-coated filter. *Rapid Commun. Mass Spectrom.* 26 (10), 1219–1231.
- Walters, W.W., Michalski, G., 2015. Theoretical calculation of nitrogen isotope equilibrium exchange fractionation factors for various NO_y molecules. *Geochem. Cosmochim. Acta* 164, 284–297.
- Walters, W.W., Michalski, G., 2016a. *Ab initio* study of nitrogen and position-specific oxygen kinetic isotope effects in the NO + O₃ reaction. *J. Chem. Phys.* 145 (22), 224311.
- Walters, W.W., Michalski, G., 2016b. Theoretical calculation of oxygen equilibrium isotope fractionation factors involving various NO_y molecules, OH, and H₂O and its implications for isotope variations in atmospheric nitrate. *Geochem. Cosmochim. Acta* 191, 89–101.
- Walters, W.W., Goodwin, S.R., Michalski, G., 2015a. Nitrogen stable isotope composition ($\delta^{15}\text{N}$) of vehicle-emitted NO_x. *Environ. Sci. Technol.* 49 (4), 2278–2285.
- Walters, W.W., Simonini, D.S., Michalski, G., 2016. Nitrogen isotope exchange between NO and NO₂ and its implications for $\delta^{15}\text{N}$ variations in tropospheric NO_x and atmospheric nitrate. *Geophys. Res. Lett.* 43 (1) 2015GL066438.
- Walters, W.W., Tharp, B.D., Fang, H., Kozak, B.J., Michalski, G., 2015b. Nitrogen isotope composition of thermally produced NO_x from various fossil-fuel combustion sources. *Environ. Sci. Technol.* 49 (19), 11363–11371.
- Williams, E.L., Grosjean, D., 1990. Removal of atmospheric oxidants with annular denuders. *Environ. Sci. Technol.* 24 (6), 811–814.
- Yoo, J.-M., Lee, Y.-R., Kim, D., Jeong, M.-J., Stockwell, W.R., Kundu, P.K., Lee, S.-J., 2014. New indices for wet scavenging of air pollutants (O₃, CO, NO₂, SO₂, and PM 10) by summertime rain. *Atmos. Environ.* 82, 226–237.
- Yu, Z., Elliott, E.M., 2017. Novel method for nitrogen isotopic analysis of soil-emitted nitric oxide. *Environ. Sci. Technol.* 51 (11), 6268–6278. <https://doi.org/10.1021/acs.est.7b00592>.